140 (2022) 213068

Contents lists available at ScienceDirect

Biomaterials Advances

journal homepage: www.journals.elsevier.com/materials-science-and-engineering-c

Lithium ion doped carbonated hydroxyapatite compositions: Synthesis, physicochemical characterisation and effect on osteogenic response *in vitro*

Nasseem Salam [a], Iain R. Gibson [a,b,*]

[a] Aberdeen Centre for Arthritis and Musculoskeletal Health, Institute of Medical Sciences, University of Aberdeen, Aberdeen AB25 2ZD, UK
[b] Department of Chemistry, University of Aberdeen, Meston Walk, Aberdeen AB24 3UE, UK

ARTICLE INFO

Keywords:
Lithium ions
Carbonate
Hydroxyapatite
Bone
Osteogenic differentiation

ABSTRACT

Hydroxyapatite is a commonly researched biomaterial for bone regeneration applications. To augment performance, hydroxyapatite can be substituted with functional ions to promote repair. Here, co-substituted lithium ion (Li^+) and carbonate ion hydroxyapatite compositions were synthesised by an aqueous precipitation method. The co-substitution of Li^+ and CO_3^{2-} is a novel approach that accounts for charge balance, which has been ignored in the synthesis of Li doped calcium phosphates to date. Three compositions were synthesised: Li^+-free (Li 0), low Li^+ (Li 0.25), and high Li^+ (Li 1). Synthesised samples were sintered as microporous discs (70–75 % theoretical sintered density) prior to being ground and fractionated to produce granules and powders, which were then characterised and evaluated *in vitro*. Physical and chemical characterisation demonstrated that lithium incorporation in Li 0.25 and Li 1 samples approached design levels (0.25 and 1 mol%), containing 0.253 and 0.881 mol% Li^+ ions, respectively. The maximum CO_3^{2-} ion content was observed in the Li 1 sample, with ~8 wt % CO_3, with the carbonate ions located on both phosphate and hydroxyl sites in the crystal structure. Measurement of dissolution products following incubation experiments indicated a Li^+ burst release profile in DMEM, with incubation of 30 mg/ml sample resulting in a Li^+ ion concentration of approximately 140 mM after 24 h. For all compositions evaluated, sintered discs allowed for favourable attachment and proliferation of C2C12 cells, human osteoblast (hOB) cells, and human mesenchymal stem cells (hMSCs). An increase in alkaline phosphatase (ALP) activity with Li^+ doping was demonstrated in C2C12 cells and hMSCs seeded onto sintered discs, whilst the inverse was observed in hOB cells. Furthermore, an increase in ALP activity was observed in C2C12 cells and hMSCs in response to dissolution products from Li 1 samples which related to Li^+ release. Complementary experiments to further investigate the findings from hOB cells confirmed an osteogenic role of the surface topography of the discs. This research has shown successful synthesis of Li^+ doped carbonated hydroxyapatite which demonstrated cytocompatibility and enhanced osteogenesis *in vitro*, compared to Li^+-free controls.

1. Introduction

Hydroxyapatite, a specific composition of calcium phosphates, remain highly investigated for applications in bone regeneration. As the most stable of calcium phosphate ceramics under physiological conditions, hydroxyapatite possess a high degree of physicochemical similarity to natural bone mineral. Nevertheless, their high stability results in reduced chemical solubility, and therefore slow resorption *in vivo*.

To augment the performance of hydroxyapatite biomaterials, researchers have investigated incorporating functional ions to enhance bone regeneration and repair. Examples of this are the substitution of strontium [1], magnesium [2] or zinc [3] ions for calcium ions, or silicate [4] or carbonate [5] ions for phosphate ions, or fluoride [6] ions for hydroxyl ions in the hydroxyapatite structure, and such substitutions have been reviewed in detail elsewhere [7,8]. A recent systematic review and meta-analysis studied the effect of inorganic supplementation of calcium phosphates on the enhancement of *in vivo* bone formation and showed strontium, magnesium and silicon supplementation specifically significantly enhanced bone repair [9].

Of interest in the present study, lithium ions (Li^+) have demonstrated osteogenic potential *in vitro* [10,11] and *in vivo* [12]; the *in vitro* studies showed osteogenic stimulation with 5–20 mM LiCl. As a non-specific

* Corresponding author at: Institute of Medical Sciences, University of Aberdeen, Foresterhill, Aberdeen AB25 2ZD, UK.
E-mail address: i.r.gibson@abdn.ac.uk (I.R. Gibson).

https://doi.org/10.1016/j.bioadv.2022.213068
Received 20 December 2021; Received in revised form 8 July 2022; Accepted 1 August 2022
Available online 3 August 2022

GSK-3 inhibitor, Li^+ induced osteogenesis is thought to involve activation of the canonical Wnt signalling pathway [13,14].

To date, there has been limited investigations into Li^+ doped hydroxyapatite/calcium phosphates in the literature. In all these studies, however, a mechanism for charge balance to account for monovalent Li^+ substituting for divalent Ca^{2+} was not introduced or proposed. This oversight may confine the accuracy of the fabrication process and the actual success of Li^+ substitution for Ca^{2+} in the crystal structure, rather than just Li^+ addition. For example, an earlier investigation mixed bovine hydroxyapatite powder with Li_2CO_3 prior to sample fabrication, however, chemical characterisation to validate the synthesis and dissolution analysis to confirm Li^+ release was absent [15]. Other studies have used a variety of precursors to introduce Li^+ as a dopant in single substitutions in hydroxyapatite or beta-tricalcium phosphate (β-TCP) including $LiNO_3$ [16–19], LiCl [20,21], Li_2O [22], and Li_3PO_4 [23], but none of these attempted to account for charge balance that would be required for successful Li^+ substitution for Ca^{2+} in the HA or β-TCP crystal lattice. On the other hand, a great deal of research has investigated carbonated hydroxyapatite owing to the presence of carbonate ions in biological apatite (~8 wt% in mammalian bone) and is thought to play an important physical and biological role [24]. The anionic carbonate ions are capable of substitution with hydroxyl ions or phosphate ions to forms A- and B-type carbonated hydroxyapatite, respectively [25]. Bone is comprised of both A- and B-type (AB-type) with a greater predominance of B-type carbonate with an A/B ratio of 0.7–0.9 [26]. Cation co-doped carbonated hydroxyapatite typically constitute sodium or ammonium ion doping owing to their predominance in the precursor chemicals (*i.e.* Na_2CO_3, $(NH_4)_2CO_3$) [7]. The co-substitution of *e.g.* monovalent sodium with carbonate ions (for phosphate ions) provides an effective method for maintaining charge balance, which single substitution of a monovalent cation for calcium does not.

To address the limitations of studies to date, this study aims to co-substitute Li^+ ions with CO_3^{2-} ions for Ca^{2+} and PO_4^{3-} ions, respectively, to achieve charge balance, resulting in novel compositions. Thus far, there has been no reported studies on Li^+ doped carbonated hydroxyapatite. To understand how Li^+ substitution affects the properties of the resulting compositions, the *in vitro* assessment of cell response, specifically the direct and indirect osteogenic response of various cell types to the samples, will be assessed.

2. Materials and methods

2.1. Sample preparation

Compositions of Li^+ doped AB-type carbonated hydroxyapatite were prepared based on an aqueous precipitation reaction, developed previously [27]. Three compositions were considered: Li^+ free (Li 0), low Li^+ substitution (Li 0.25), and high Li^+ substitution (Li 1). Carbonate and Li^+ were co-substituted in adherence with Eq. (1), where 0, 0.25, and 1 correspond to the value of *x*; quantities of respective reactants were calculated to generate an approximately 0.025 mol (25 g) of material, and the masses used are listed in Table S1. For all compositions, carbonate was introduced into the synthesis by bubbling CO_2 gas into the phosphoric acid solution prior to precipitation reaction, whereas the Li substituted compositions had an additional source of carbonate ions from the lithium carbonate (Li_2CO_3) reactant used. This proposed mechanism does not account for carbonate substitution on the hydroxyl site, which could occur by a mechanism independent of *x*.

$$(10-x)Ca^{2+} + xLi^+ + (6-x)PO_4^{3-} + xCO_3^{2-} + 2OH^- \rightarrow Ca_{10-x}Li_x(PO_4)_{6-x}(CO_3)_x(OH)_2 \quad (1)$$

For Li^+ doped compositions, Li_2CO_3 (255823, Sigma Aldrich, UK) was included in the calcium hydroxide (10304KA, VWR, UK) suspension preceding acid addition. In a typical synthesis, phosphoric acid (EMSURE 85 % assay, Merck, UK) in 250 mL of carbonated distilled water – achieved by bubbling CO_2 gas for 30 min prior – was added dropwise to a 250 mL calcium hydroxide suspension in distilled water under continuous stirring and alkaline conditions (pH > 10, *via* the addition of 50 mL of concentrated ammonium hydroxide). Upon addition of all of the acid solution, the reaction was stirred for 2 h prior to aging unstirred for a further 24 h. Following aging, the mixture was filtered under vacuum utilising Whatman® grade 3 filter paper with the ensuing filter-cake dried at 80 °C overnight and then, ground finely using a mortar and pestle.

To produce discs for sintering, approximately 300 mg of powder was pressed into a Ø 13 mm die set and a 1 ton force applied for 1 min using a hydraulic press. Produced discs were sintered in a tube furnace (Model STF 15/450 with 3216 controller; Carbolite, UK) under a CO_2 rich environment with CO_2 gas flowing into distilled water and then the furnace at 500 cm^3/min. The heat treatment involved ramping up to the required temperature at 2.5 °C/min, holding for 1 h, and a cooling rate of 10 °C/min. Sintering temperatures of 1150 °C, 950 °C, and 750 °C were used for Li 0, Li 0.25, and Li 1, respectively, as experimentation identified that these temperatures allowed fabrication of discs with similar sintered density (data not shown). Sintered densities were determined from the masses and dimensions of the sintered discs, and were expressed as a percentage of the theoretical density of hydroxyapatite [28]. As sintering samples in a CO_2 atmosphere can lead to partial substitution of hydroxyl groups for carbonate groups in the HA structure, all three compositions were sintered in the CO_2 rich environment to provide consistency. To generate samples with a higher surface area and thus, greater ion release, sintered discs were ground and sieved and fractionated to 500–1000 μm to produce granules or <200 μm to produce powder samples.

2.2. Powder X-ray diffraction

The crystalline phases of powder samples were identified using an X'Pert Pro diffractometer (PANalytical Ltd., UK) operating at 45 kV and 40 mA using Cu K_α radiation (λ = 1.5418 Å). X-ray diffraction (XRD) patterns were collected from 10 to 80° 2θ with a step size of 0.01313° and time per step of 998.07 s. Confirmation of a hydroxyapatite phase was obtained by comparing experimental patterns with the ICDD standard pattern of HA (PDF Card No. 9-432 [28]). Unit cell parameters were calculated using unit cell refinement in HighScore Plus software, using the space group $P6_3/m$ and unit cell parameters and reference peak positions from the ICDD standard pattern of HA as a starting point for the refinement. The crystallinity of the sintered samples was determined by the method described be Landi et al. [29].

2.3. Fourier transform infrared spectroscopy

Fourier transform infrared (FTIR) spectra were obtained of the powder samples. The absorbance was measured between 4000 and 400 cm^{-1} at a 2.0 cm^{-1} resolution with 8 scans using a Spectrum Two FTIR spectrometer (Perkin-Elmer, UK) equipped with a Diamond/ZnSe ATR crystal. The Solver add-in in Microsoft Excel was employed for composite peak deconvolution of the carbonate ν_2 region and the phosphate ν_4 region of the Li 1 sample heated at 750 °C, using Gaussian profiles.

2.4. Specific surface area determination

The specific surface areas of powder samples were determined using a Micromeritics Tristar 3000 surface area analyser. Samples were pre-heated at 200 °C under flowing N_2 gas prior to collection of isotherms for calculation using the BET method. Due to the low surface area of the samples, multipoint analysis to calculate BET surface area could not be performed, so only a single point (at a partial pressure of ~0.2) BET method was used.

2.5. Contact angle measurement

The surface contact angle of sintered discs was measured using a FTA1000 B sessile drop instrument (First Ten Ångstroms, USA). A 5 μL droplet of distilled water was manually dispensed using a Gilmont goniometer and the resultant contact angle measured using the corresponding Fta32 software (First Ten Ångstroms, USA). Measurements were taken at ambient temperature and humidity using 3 discs per composition for each sintering temperature.

2.6. Scanning electron microscopy

Observations of surface topography, microporosity, and grain morphologies was performed using a Zeiss EVO MA10 scanning electron microscope employing a 10 kV accelerating voltage (Carl Zeiss, UK). Samples were mounted on aluminium stubs using carbon adhesive tabs and silver paint was added to form conductive paths between the samples and the stubs. Mounted samples were coated with an approximately 10 nm gold/palladium mixture prior to imaging.

2.7. Dissolution studies

To investigate the ionic release from the synthesised Li^+ doped carbonated hydroxyapatite samples and/or changes in the soaking solution ion composition, each of the three compositions (Li 0, Li 0.25, and Li 1) were prepared as sintered discs, granules, and powders and soaked in a 0.08 M acetic acid-sodium acetate buffer solution (pH 5.5) [30] or Dulbecco's modified essential media (DMEM) in triplicate. The concentration of material per soaking volume for granules and powders was kept at 1.5 mg/mL as previously recommended [31], whilst the volume used for discs was calculated based on the apparent surface area as set out by ISO 23317. For DMEM experiments, granule and powder samples were soaked in a total volume of 20 mL, whilst samples in the acetate buffer were soaked in a total volume of 35 mL. Samples in the acetate buffer or DMEM were incubated at 25 °C/300 RPM or 37 °C/120 RPM, respectively. Experiments in DMEM involved complete replenishment with fresh solutions at timepoints, whereas for samples in acetate buffer aliquots of 1 mL were taken at timepoints and replaced with fresh acetate buffer. Upon endpoint, test samples were washed in ethanol, air dried, and stored in a desiccator prior to preparation for SEM imaging as per the previous section.

The soaked solutions were analysed for Ca^{2+} and Li^+ using microwave plasma – atomic emission spectroscopy (MP-AES), whilst phosphate ions were measured using a previously described colorimetric assay [32]. For measurement of Ca^{2+} and Li^+, test samples were diluted 10-fold with 1 % (v/v) HNO_3 in deionised water prior to triplicate measurements using an Agilent 4100 instrument at the following wavelengths: 393.366 nm for Ca^{2+} and 670.784 nm for Li^+. For measurement of phosphate ions, 20 μL aliquots of test samples was added, in triplicate, to a 96 well microwell plate prior to the addition of 200 μL test reagent comprised of 1 part 4.2 % (w/v in 4 M hydrochloric acid) ammonium molybdate tetrahydrate and 3 parts 0.045 % (w/v in deionised water) malachite green oxalate salt. After a 15 min incubation, the absorbance was read at 650 nm using a BioTek Synergy HT microplate reader.

2.8. Chemical analysis of powders

The bulk composition of the powder samples was determined by dissolving 12.5 mg of powder in 100 mL of 1 % HNO_3 and measuring the Ca^{2+} and Li^+ and phosphate concentrations as per the previous section. Ca^{2+} and Li^+ measurements using MP-AES were taken following a 100-fold dilution in 1 % HNO_3 whilst, a 20-fold dilution was employed prior to the colorimetric phosphate assay.

The carbonate content of the powder samples was determined using a LECO CS744 carbon/sulphur analyser (LECO Instruments UK Ltd., UK). For each sample, duplicate measurements were made and the mean value reported alongside the standard deviation.

2.9. Cell culture

C2C12 cells, human osteoblast (hOB) cells, and human mesenchymal stem cells (hMSCs) were purchased from the American Type Culture Collection (*via* LGC standards, UK), PromoCell (Germany), and AllCells (USA), respectively. Cells were maintained in routine culture conditions using: high glucose DMEM with 10 % FBS and 4 mM L-glutamine for C2C12 cells, Gibco™ low glucose DMEM containing pyruvate with 10 % FBS, 5 μg/mL ascorbic acid 2-phosphate, 1 % non-essential amino acids, and 1 % penicillin/streptomycin for hOB cells, and high-glucose DMEM with 10 % FBS, 2 mM L-glutamine, and 1 % penicillin/streptomycin for hMSCs.

Supplementation with 10 nM dexamethasone, 10 mM β-glycerophosphate, and 50 μM ascorbic acid 2-phosphate (hMSCs only) was used as a positive osteogenic control for hOB cells and hMSCs. As an additional control, to examine the effects of only Li^+, cells were treated with 10 mM LiCl (in PBS).

2.10. Resazurin assay

The resazurin assay was used to indirectly monitor any cytotoxic effects of the sintered discs. C2C12 cells (40,000 cells/cm^2) and hOB cells and hMSCs (20,000 cells/cm^2) were seeded in a 100 μL volume onto the discs and allowed to adhere for 4 h. Cells were maintained in culture for 7 days with measurements taken at day 3 and 7.

2.11. Osteogenic differentiation

To evaluate the influence of the synthesised discs on osteoinduction and osteoblast functionality, C2C12 cells, hMSCs, and hOB cells were seeded per the previous section and cultured for 7 days prior to measurement of ALP activity. This marker was chosen as it has been shown to be a good predictor of bone forming capacity of MSCs *in vivo* [33] and of correlating C2C12 cell osteogenic differentiation in response to doses of BMP-2 from demineralised bone matrix, and bone formation *in vivo* [34].

Owing to the response observed in hOB cells, two sets of experiments were performed to distinguish the effects of the discs' topography from their surface chemistry. A set of discs were manually polished to remove the effects of the topography using abrasive paper, whilst another set of discs were sputter coated with a gold/palladium mixture to insulate the seeded cells from the underlying ionic effects.

In order to ascertain whether the dissolution products of the synthesised materials were able to induce osteogenesis, sintered discs, granules, and powders were soaked in 5 mL DMEM for 7 days at 37 °C. The mass of granules and powders used was standardised to the mass of the discs (~300 mg) for a final concentration of 60 mg/mL. After the 7 days soaking, the culture media was sterile filtered, supplemented to obtain growth media, and used to culture C2C12 cells for 7 days prior to measurement of ALP activity. Moreover, the sintered materials were evaluated in an insert culture setup which ensured C2C12 cells responded to the dynamic effects of the materials within the culture media. The sintered granules were considered as they provided a greater ionic release compared to discs whilst remaining fixed in position compared to the powders. Three concentrations were evaluated, 15, 30, and 60 mg/mL, for a 7-day culture prior to measurement of ALP activity. Furthermore, positive responses from these experiments were authenticated in hMSCs.

2.12. Statistics

For *in vitro* characterisation, 3 discs per composition were evaluated in each experiment, with experiments performed in triplicate. Statistical

analysis was carried out using GraphPad Prism 7.04 (California, USA) with assessment of statistical differences between multiple conditions using one-way analysis of variance with a post-hoc Tukey's test. Results are presented as mean ± standard deviation (SD); p values < 0.05 were considered statistically significant. For graphical presentation, * indicates $p < 0.05$, ** indicates $p < 0.01$, and *** indicates $p < 0.001$.

3. Results

3.1. Physicochemical characterisation

With the exception of Li 1, samples synthesised were phase-pure, showing only X-ray diffraction peaks corresponding to an HA phase (Fig. 1A); for Li 1 samples a small calcite impurity phase was detected by a single diffraction peak at 29.4°2θ. The determined unit cell parameters indicated modest changes; comparisons of a and c unit cell parameters suggested negligible difference between Li 0 and Li 0.25 samples, whilst Li 1 samples illustrated a slight reduction in both a and c unit cell parameters compared to the other samples, Table 1. Likewise, similar observations were found with respect to the volume of the unit cell. The crystallinities of all samples were calculated as being >95 %.

Infrared spectra showed the typical vibrations previous reported data on AB-type carbonated hydroxyapatite in the literature, with the spectrum for the Li 1 sample between 400 and 1800 cm^{-1} shown in Fig. 1B [35,36]. Only a weak vibration at approximately 3569 cm^{-1}, corresponding to hydroxyl group stretching, was observed at wavenumbers above 1800 cm^{-1} so spectra are only plotted for the region below this. Typical bands for carbonate groups were observed in all samples at approximately 1540, 1497, 1450, 1412 and 1350 cm^{-1} for ν_3 vibrations, with the Li 1 sample showing an additional peak at approximately 1381 cm^{-1}. Deconvolution of the carbonate ν_2 and the phosphate ν_4/hydroxyl libration regions of the sample with the highest carbonate content (Li 1) provided a clearer overview of the carbonate substitution (Fig. 2). The carbonate ν_2 region could be fitted to three peaks corresponding to A-type, B-type and labile carbonate (Fig. 2A), although the region relating to labile carbonate (850–865 cm^{-1}) does not fit very well to a single peak suggesting slightly different environments for labile carbonate. A clear OH libration peak at approximately 630 cm^{-1} was observed (Fig. 2B), with 3 peaks corresponding to apatitic phosphate ν_4 vibrations and a peak at approximately 532 cm^{-1} that has been assigned to HPO_4 groups.

Table 1
Physicochemical characterisation of Li^+ free (Li 0) and Li^+ doped (Li 0.25 and Li 1) carbonated hydroxyapatite samples. Contact angle and sintered density values are listed as mean values, with standard deviations in brackets.

	Li 0	Li 0.25	Li 1
a-Axis[a] (Å)	9.418 (1)	9.418 (1)	9.4086 (9)
c-Axis[a] (Å)	6.878 (2)	6.878 (1)	6.870 (1)
SSA[b] (m^2/g)	0.14	0.21	0.31
Contact angle (°)	58.7 (5.1)	59.9 (2.2)	63.0 (2.8)
Sintered density (%theor)	72.8 (3.4)	75.9 (1.3)	71.2 (1.9)

[a] Values in brackets refer to the calculated e.s.d from the refinements.
[b] Values were calculated using a single point BET method.

SEM micrographs of the sintered discs portrayed heterogeneous porosity and grain attributes between the compositions examined (Fig. 1C). Li 0 discs possessed a polygonal grain shape with variable pore and grain sizes. In contrast, Li 0.25 discs displayed two classes of grain shape: grains comparable to Li 0 discs and the other more elongated and cylindrical with the latter retaining a relatively uniform size. Li 1 discs displayed predominantly elongated, cylindrical grains with greater uniformity compared to the other compositions, although Li 1 discs

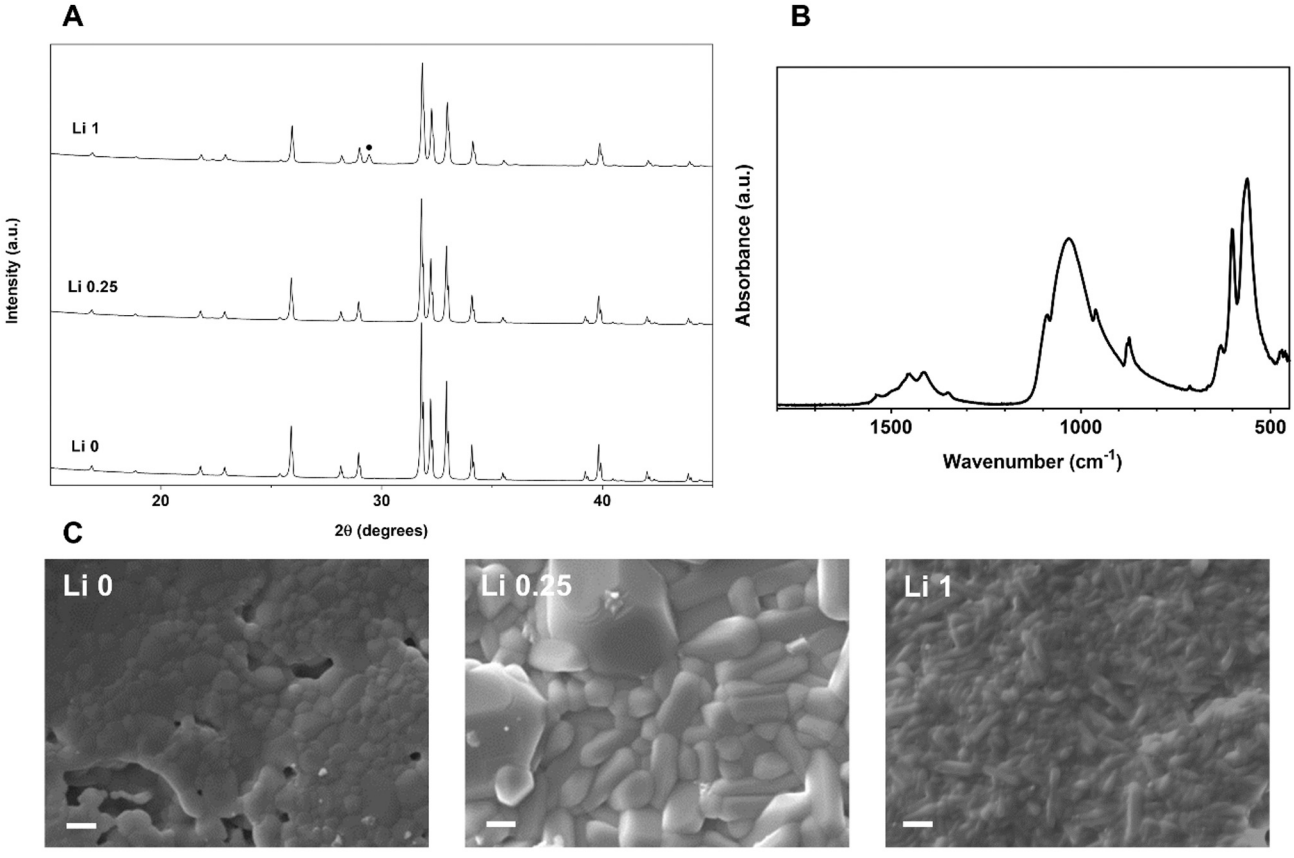

Fig. 1. XRD patterns (A) and SEM micrographs (C) of Li 0, Li 0.25, and Li 1 samples. FTIR spectrum of Li 1 samples (B). Diffraction peaks attributed to calcite are denoted by ●. Scale bars in (C) correspond to 2 μm.

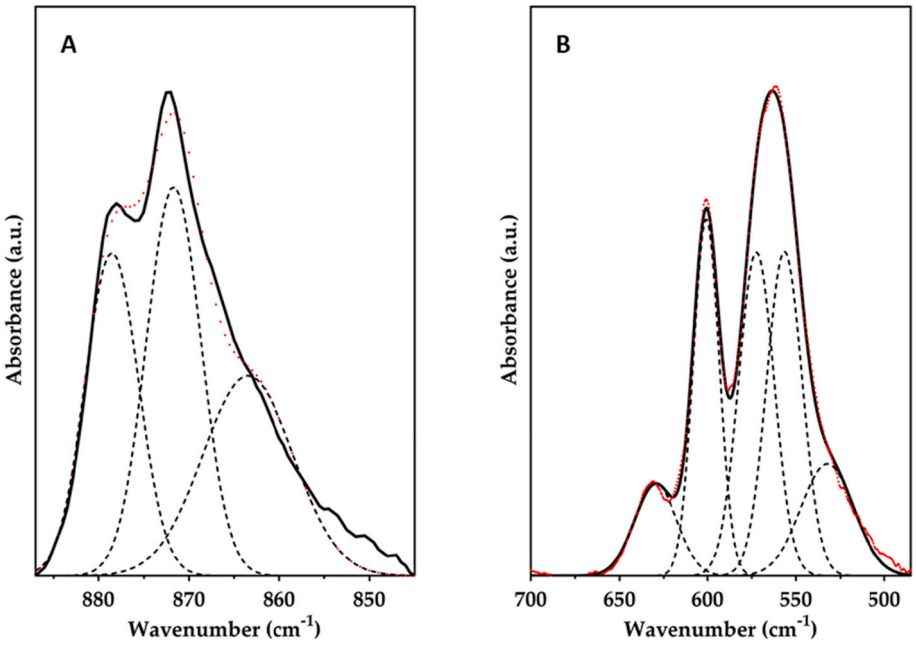

Fig. 2. Deconvolution of the FTIR spectrum for the CO_3 ν_2 (A) and PO_4 ν_4 (B) regions of Li 1 sample heated to 750 °C. Dashed lines correspond to the individual fitted peaks, the solid black line corresponds to the fitted model spectra, and the red data points correspond to the acquired experimental data. (For interpretation of the references to colour in this figure legend, the reader is referred to the web version of this article.)

depicted variable pore sizes. SEM images of granules and powders (data not shown) showed irregular shaped particles with dimensions within the sieved ranges of each.

Calculation of sintered densities of sintered discs indicated general parity between compositions as per optimisation of sintering temperature, with mean values ranging from 71.2 to 75.9 % of the theoretical density (the mean actual sintered densities for Li 0, Li 0.25 and Li 1 were 2.30, 2.39 and 2.25 g/cm^3, respectively). Likewise, this effect was reflected in the contact angle measurements, with values showing a small, but not significant, increase with increasing Li substitution. Measurements of the specific surface area of Li 0, Li 0.25, and Li 1 powders are given in Table 1. A general trend of increased specific surface area of the powders with increased Li^+ doping is observed. However, it should be noted the different sintering temperatures used for these samples (1150, 950, and 750 °C for Li 0, Li 0.25, and Li 1 samples, respectively).

Elemental analysis of the chemical composition of the powders, using MP-AES (Ca and Li) and a colorimetric assay (P) showed that the Ca/P and (Ca + Li)/P molar ratios increased with increasing Li^+ substitution, consistent with the design compositions from Eq. (1) that require increasing carbonate substituting on the phosphate site (B-type), Table 2. The measured Li^+ content in the samples, quoted as a mol% of Li^+ compared to the total moles of cations (Ca + Li), was close to the designed compositions of 2.5 mol% Li and 10 mol% Li for Li 0.25 and Li 1, respectively. The measured carbonate contents of the samples showed that the Li^+ free (Li 0) sample and the low Li^+ (Li 0.25) samples had comparable quantities of carbonate, with the high Li^+ composition (Li 1) having approximately four times the carbonate content, consistent with the difference in the level of Li^+ substitution.

Table 2
Chemical analysis of Li^+ free (Li 0) and Li^+ doped (Li 0.25 and Li 1) carbonated hydroxyapatite powders; results are reported as mean values with standard deviations in brackets.

	Li 0	Li 0.25	Li 1
Ca/P[a]	1.61 (0.04)	1.63 (0.01)	1.68 (0.06)
(Ca + Li)/P[a]	1.61 (0.04)	1.67 (0.01)	1.85 (0.07)
Li (mol%)[a]	0 (0.00)	2.53 (0.02)	8.81 (0.03)
CO_3 (wt%)[b]	2.04 (0.01)	2.06 (0.02)	7.99 (0.10)

[a] Ca and Li values determined by MP-AES analysis and P values determined by a colorimetric phosphate assay. Li content reported as mol% of the cations, Li/(Ca + Li).
[b] CO_3 values determined by combustion analysis.

3.2. Dissolution behaviour of sintered powders, granules and discs

Measurement of Ca levels in DMEM after incubating samples illustrated several trends with respect to differences between compositions and the form of material evaluated. As expected, powders resulted in greater consumption of calcium ions from the media, as a result of surface precipitation of a CaP layer, followed by granules and then discs (Supplementary Fig. S1B, A, and Fig. 3A, respectively). Considering the continuous exchange of media at timepoints, findings indicated sustained consumption of calcium for the duration of the timepoints examined. Although the progression of Ca consumption remained similar between the compositions, the data highlighted slight differences in relation to one another, and these were more evident for incubating granules and powder, rather than the granules. The granules upheld increased consumption of Ca up to day 14 which then plateaued from day 21 (Fig. 3A). For P measurements, Li 0 granules demonstrated a sustained increase in P consumption throughout the soaking period whilst Li 0.25 and Li 1 granules began to plateau at day 14, although, increased depletion was observed with Li 1 granules at day 28 (Fig. 3C). Data from Li^+ measurements indicated a burst release profile for the Li^+ doped compositions regardless of the form of material evaluated. As expected, Li 1 granules demonstrated a higher Li release compared to Li 0.25 granules with an approximately 6-fold increase at day 1 (Fig. 3E). Following a sharp incline at day 1 for all samples, pH levels remained stable throughout the soaking period (Supplementary Fig. S2); dissolution experiments were not performed in a CO_2 enriched atmosphere, resulting in the initial pH increase observed in the first 24 h.

In general, the solubility of granules in the acetate buffer was dependent on the design substitution value with greater Ca, P, and Li release per increased Li^+ substitution with Ca and P release from Li 0.25 granules closely following the results of the Li 1 granules (Fig. 3B, D). Furthermore, a burst Li^+ release was observed for Li 0.25 and Li 1 granules which began to plateau at an earlier stage in Li 0.25 granules

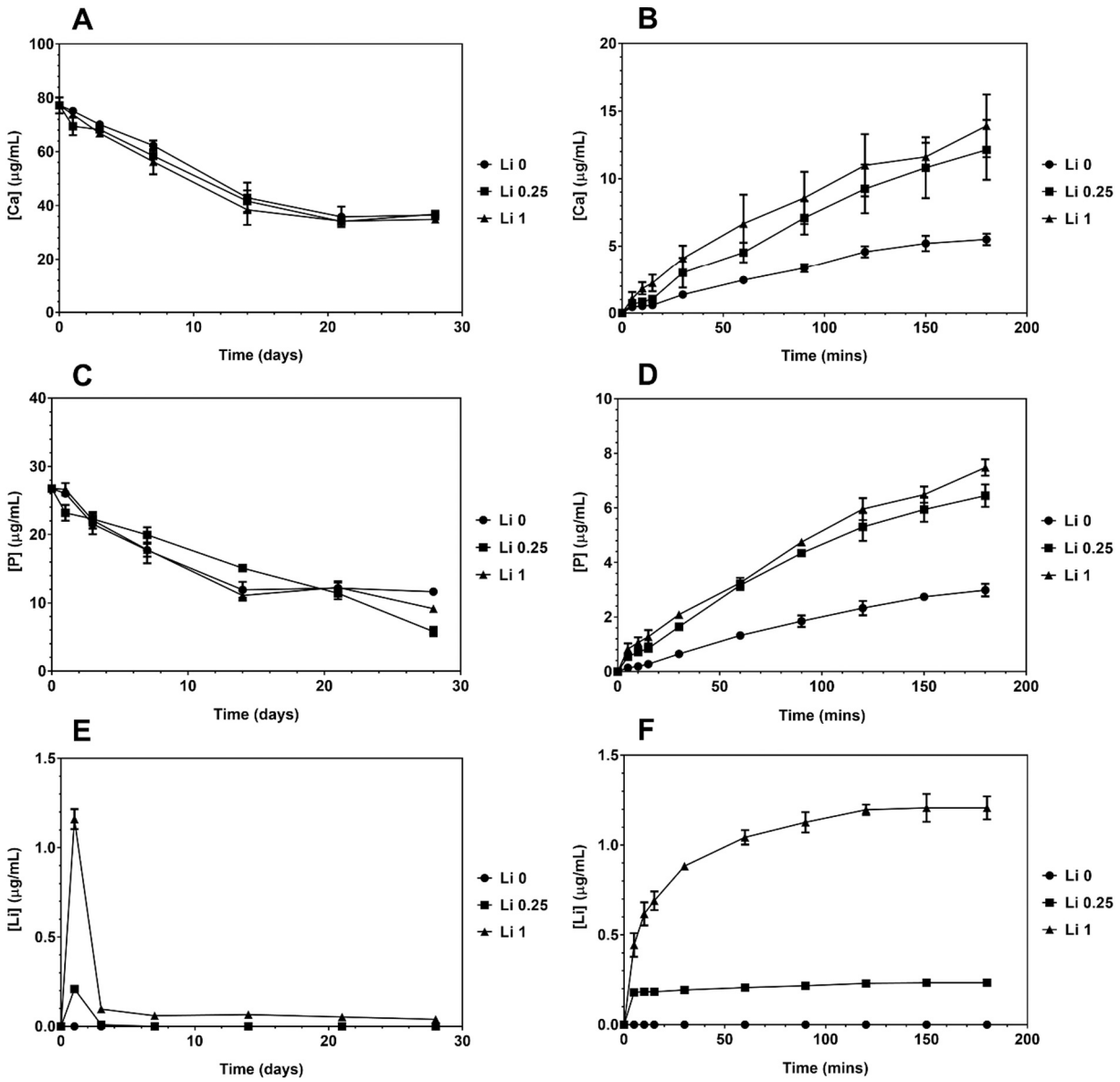

Fig. 3. Dissolution profiles of Li 0, Li 0.25, and Li 1 granules in DMEM (A, C, E) and acetate buffer (B, D, F).

compared to Li 1 granules (Fig. 3E). The burst release profile for Li reaffirmed data from DMEM experiments but differed from the Ca and P findings in the acetate buffer which depicted a sustained release of these elements throughout the soaking period.

To confirm calcium phosphate precipitation on the surface of materials following incubating in DMEM, SEM micrographs were taken post-dissolution to visualise the surface for apatite formation (Fig. 4). Observations proved challenging, particularly at higher resolutions, with indications of charging effects presumably due to an air gap resulting from the separation of the comprehensive precipitation layer and the underlying surface of the disc. Indeed, visualisation of granules following DMEM experiments indicated widespread bulbous surface morphology characteristic of apatite formation.

3.3. *In vitro osteogenesis in response to dissolution products*

Treatment with conditioned media, derived from incubating discs, granules, and powders, failed to induce a significant increase in C2C12 cell ALP activity with the exception of Li 1 powders ($p < 0.0001$) which generated a greater response than a positive control of 10 mM LiCl stimulation (Fig. 5A). The Ca concentrations in the conditioned media for each composition/sample type was measured (Fig. 5B) and does not show a clear correlation with the corresponding ALP activity. To confirm whether the aforesaid response was a result of Li^+ release, a lower (30 mg/ml) and higher (90 mg/ml) mass of Li 1 powders was soaked prior to use in culture. Findings demonstrated a proportional increase in ALP activity with increased Li 1 powder concentration (Fig. 5C). Ca concentrations in the conditioned media were also measured for each composition, sample type and also powder concentration used for Li 1 (Fig. 5D). Although the Ca concentration varied significantly for the different compositions and sample type tested, consistent with the dissolution data in Fig. 3 and Supplementary Fig. S1, when different powder concentrations of Li 1 were used to produce conditioned media the Ca concentration in these media were comparable, but the ALP activity values were significantly different. Analysis of ALP activity upon exposure to sintered granules held within inserts demonstrated a Li^+ specific osteogenic response (Fig. 5E). Li 0 granules failed to induce a significant response regardless of concentration examined ($p = 0.9997$ at 15 and 60 mg/mL, and $p > 0.9999$ at 30 mg/mL). In contrast, Li 1 granules prompted a significant increase in ALP activity for all

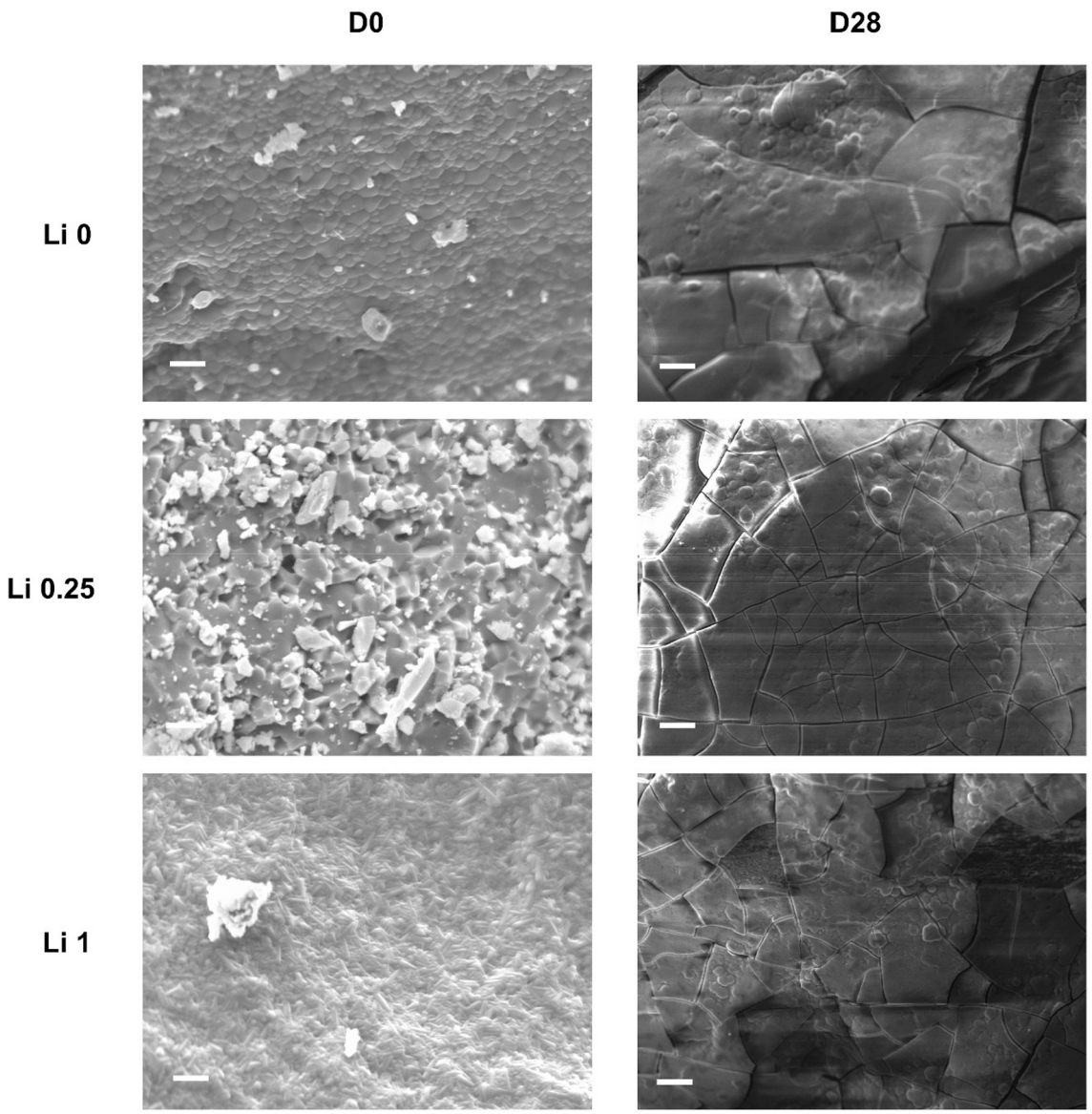

Fig. 4. SEM micrographs of the surface of Li 0, Li 0.25, and Li 1 granules (0.5–1 mm size) prior and post soaking in DMEM for 28 days. Scale bars equate to 2 μm.

concentrations studied, albeit levels peaked at 30 mg/mL ($p = 0.0002$ at 15 mg/mL, and $p < 0.0001$ at 30 and 60 mg/mL). The Ca concentration in the media showed an increase with increased incubation time of the granules within the culture inserts, with the Li 0 granules resulting in a slightly greater Ca increase (Fig. 5F).

The positive response illustrated in C2C12 cells were further authenticated in hMSCs. For this experiment, conditioned media from Li 1 powders (60 mg/mL) and 30 mg/mL Li 1 granules in inserts were assessed, compared to corresponding Li 0 powders and granules. Fig. 6A demonstrated a significant induction of ALP activity upon treatment with the conditioned media ($p < 0.0001$) and the granules ($p = 0.0028$). In contrast to C2C12 cells, conditioned media from Li 1 powders did not generate a greater response than LiCl treatment. The Ca, P and Li ion concentrations in the media of these experiments were measured, giving an indication of the ion release or CaP precipitation that occurred during the incubation of the granules in the cell culture wells. The Li^+ release was greater from powders than granules, consistent with the dissolution experiments, but the Li^+ concentrations achieved were significantly higher than from the dissolution experiments (Fig. 6D). Incubating the granules within the cell cultures did not result in the large consumption of Ca and P from the media that was observed in the dissolution experiments (Fig. 6B & C), but the concentrations used were very different in these two experiments.

3.4. In vitro response to sintered discs

In both hOB cells and hMSCs, Li 1 discs caused faster cell spreading compared to Li 0 and Li 0.25 discs with recognisable cell polarisation within 4 h and the typical fibroblast-like morphology (Fig. 7). In contrast, cells on Li 0 and Li 0.25 discs remained predominantly rounded albeit with extensive cell projections (filopodia) indicative of the onset of cell polarisation. At 24 h, hOB cells and hMSCs exhibited cell spreading regardless of disc composition with no noticeable differences in cell morphology.

A significant increase in ALP activity was observed in C2C12 cells seeded onto the sintered discs across all the compositions evaluated compared to cells in the growth media control ($p = 0.0007$ for Li 0, $p = 0.0006$ for Li 0.25, and $p < 0.0001$ for Li 1) (Fig. 8A). A similar trend to C2C12 cells was observed in hMSCs (Fig. 8C), although, differences in the level of statistical significance was detected. In contrast to C2C12 cells, only Li 1 discs induced a significant difference in ALP activity compared to the growth media control with an over 3-fold increase ($p =$

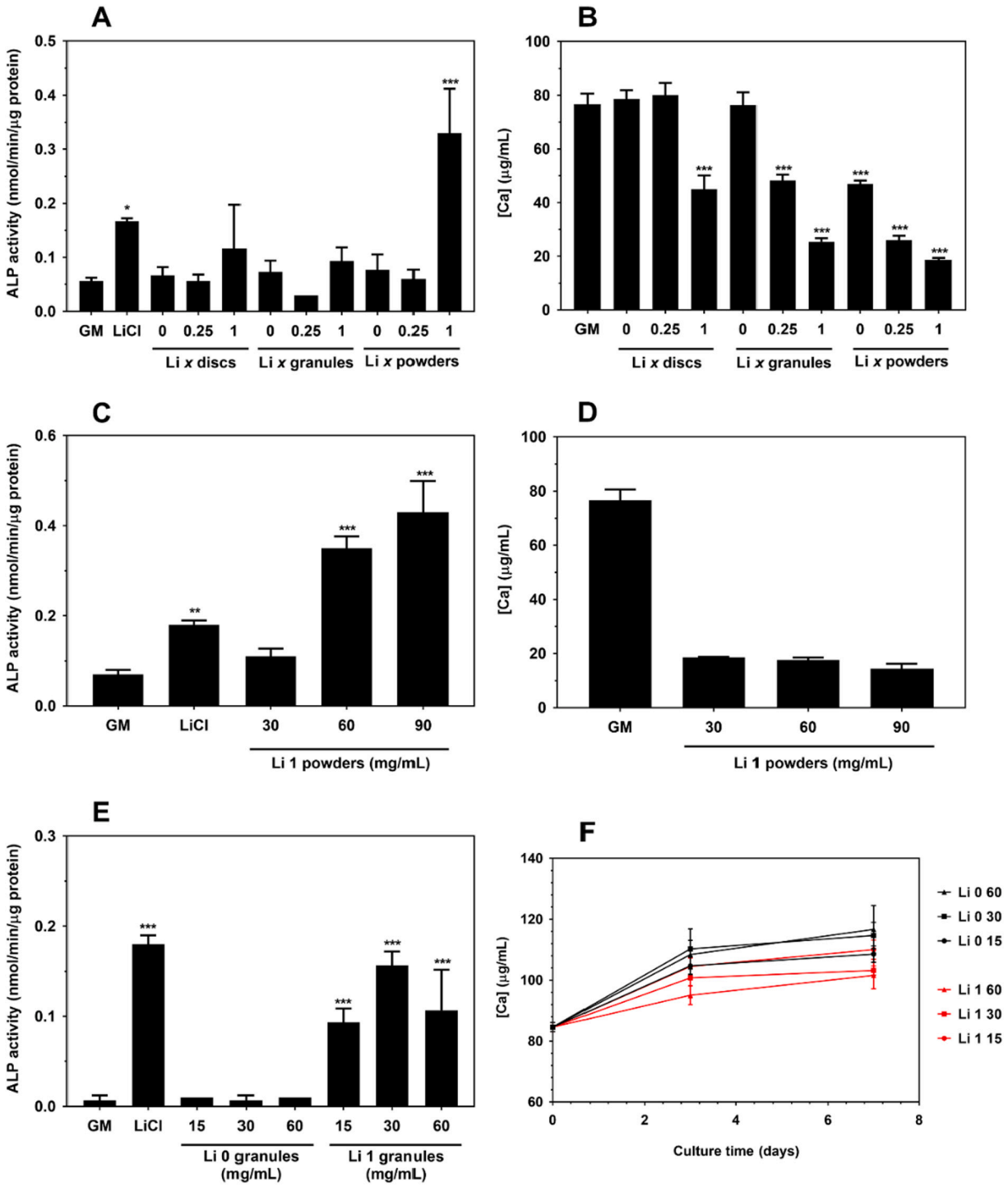

Fig. 5. ALP activities of C2C12 cells (A, C, E) with corresponding measurement of Ca concentrations in the media (B, D, F). Cells cultured in conditioned media derived from a 7 day soaking of discs, granules, and powders at 60 mg/mL (A, B). Cells cultured in conditioned media derived from a 7 day soaking of Li 1 powders at 30, 60, or 90 mg/mL (C, D). Cells cultured with granules held within inserts at 15, 30, or 60 mg/mL (E, F).

0.0004). Exposure to Li^+ doped carbonated hydroxyapatite failed to induce a significant response in hOB cells compared to cells in the growth media control (Fig. 8E). However, cells seeded onto the Li 0 discs generated a significant increase in ALP activity ($p < 0.0001$). Moreover, a proportional relationship of decreased ALP activity with increased Li^+ substitution was observed.

Generally, findings demonstrated C2C12 cells, hOB cells, and hMSCs seeded onto discs retained comparable growth to cells in the growth media control, with no significant changes in mitochondrial activity with culture time (Fig. 8B, E, F). Overall, findings illustrated sintered discs retained cytocompatibility for all the compositions analysed regardless of the cell type considered.

3.5. *Influence of surface topography on hOB cell differentiation*

To evaluate the influence of the surface topography on hOB cells, two experiments were considered. Firstly, to abrogate the underlying surface chemistry but retain the overall surface topography, discs were sputter

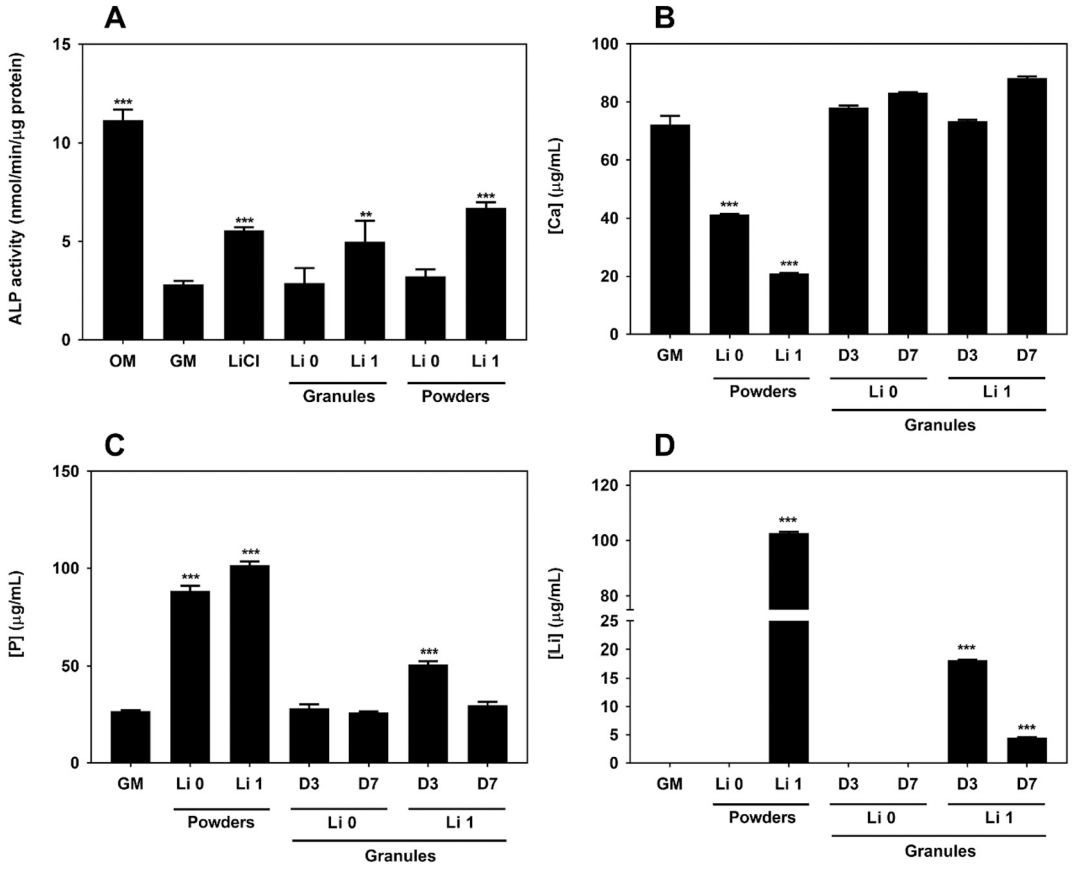

Fig. 6. ALP activities of hMSCs cultured in Li 0 and Li 1 granules held within inserts at 30 mg/mL or conditioned media derived from a 7 day soaking of Li 0 and Li 1 powders at 60 mg/mL (A). Corresponding measurements of Ca (B), P (C), and Li (D) in the media are presented.

coated with gold/palladium, as per SEM preparation. Measurement of calcium ion levels, from media collected during culture, authenticated the experimental setup which masked ion release from the sintered discs. Findings from these experiments demonstrated a significant increase in ALP activity in coated Li 0 and Li 0.25 discs compared to the growth media control ($p = 0.0422$ and $p = 0.0166$, respectively) (Fig. 9A). In contrast, although a 2-fold increase was measured in Li 1 discs, no statistical significance was detected. Nevertheless, additional analysis indicated no difference in ALP activity of cells between Li 1 discs and those of the other compositions. Sputter coating of the discs led to no changes in the Ca concentration of the culture media (Fig. 9B).

In a complementary experiment, sintered discs were polished to generate a uniform surface, and thereby, remove the influence of the surface topography. Here, hOB cells remained unresponsive with no noticeable increase or decrease in ALP activity measured, regardless of composition examined ($p < 0.9999$) (Fig. 9C); polished surfaces of all discs appeared similar by SEM (Fig. 9D).

4. Discussion

The aim of this study was to address a significant deficiency in previous studies that have attempted to substitute Li^+ ions into hydroxyapatite or tricalcium phosphates, which has been the exclusion of a charge balancing mechanism for the designed Li^+ for Ca^{2+} ion substitution. To achieve this, we performed a co-substitution of Li^+ and CO_3^{2-} ions for Ca^{2+} and PO_4^{3-} ions in hydroxyapatite using an aqueous precipitation method. This approach produced compositions with a low or a high concentration of Li^+ ions, allowing us to identify the effect of these compositions on their physical, chemical and biological properties, compared to a Li-free control prepared in a similar manner.

In determining the mechanism for the physicochemical changes observed in the samples studied, several factors are of significance including the sintering conditions (time, temperature, gaseous environment) and precursor concentrations (particularly Li^+ and carbonate). Notably, previous investigations into sintering parameters in carbonated hydroxyapatite demonstrated densification from 700 °C [37], whereas stoichiometric hydroxyapatite typically exhibits densification from 800 to 900 °C [23]. Although heat treatments are considered isochronal, this fails to take into account the ramp-up process which may result in samples undergoing densification for several hours prior to reaching the sintering temperature. Results from density measurements indicated improved sinterability (*i.e.* lower temperatures required for densification) with increased Li^+ doping. Doping of β-tricalcium phosphates using Li_2O as a precursor illustrated minimal differences in bulk and apparent density with increased dopant and no apparent trend [22]. In contrast, commercial hydroxyapatite powders doped with $LiNO_3$ resulted in moderate increased densities in Li 0.2 and 0.4 (wt%) samples but markedly reduced densities in Li 0.6 (wt%) samples [16]. Preceding work has demonstrated carbonate as paramount for sintering improvement in pure carbonated hydroxyapatite with carbonated water and heat treatment under a CO_2 rich environment as the sources of carbonate ions [35]. Thus, the improved sinterability observed in the present study is caused by increased carbonate ions derived from Li_2CO_3, and also CO_2 present in the sintering atmosphere.

Changes to the crystal structure of hydroxyapatite are caused by an aggregate of the relative incorporation of Li^+, A-type carbonate, and B-type carbonate ions, and sintering temperature. Formation of A-type carbonated hydroxyapatite is generally agreed to expand the *a* axis length and contract the *c* lattice parameter as CO_2 reacts with two hydroxyl groups to form carbonate resulting in reduced occupancy in the hexagonal channel [38]. Whilst, the inverse is true for B-type carbonated hydroxyapatite as the smaller planar carbonate substitutes the larger

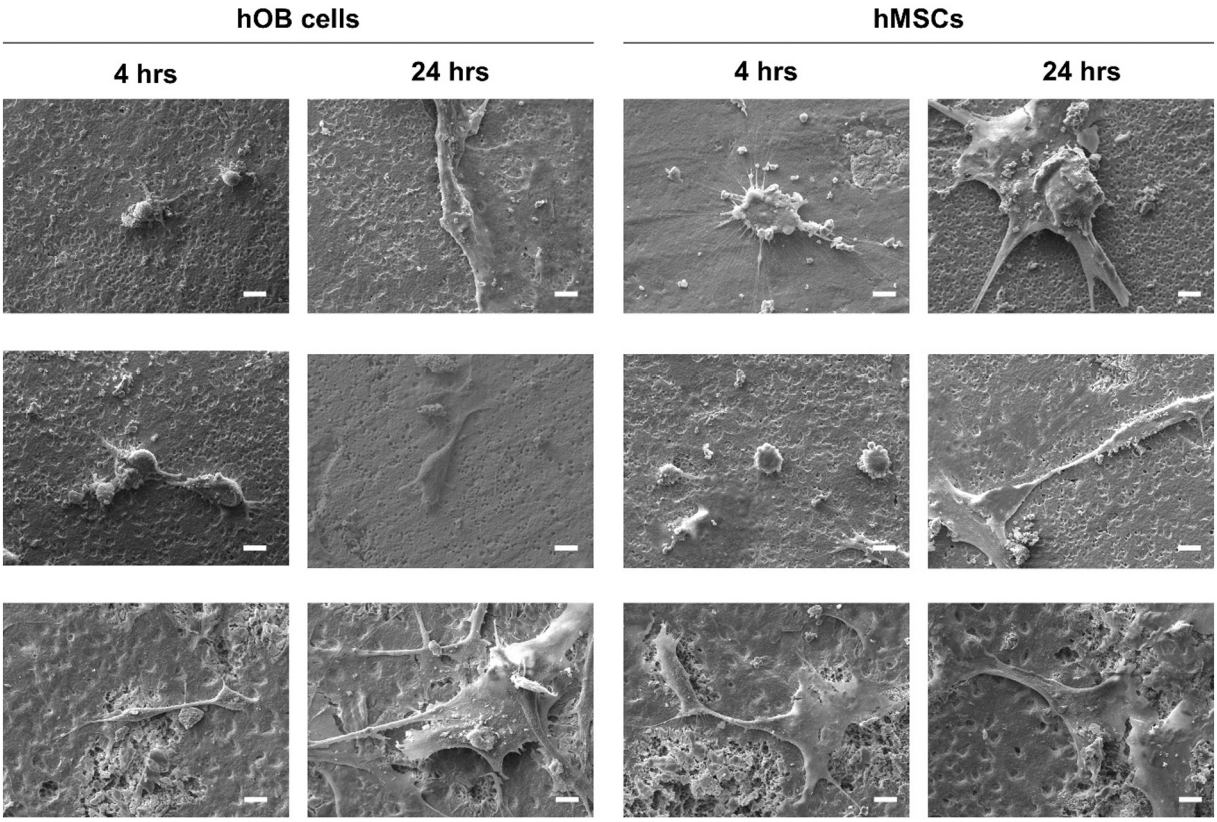

Fig. 7. SEM micrographs of hOB cells and hMSCs cultured on Li 0 (top row), Li 0.25 (middle row), and Li 1 discs (bottom row) for 4 h and 24 h. The scale bar corresponds to 10 μm.

tetrahedral phosphate [39]. On the other hand, much of the data on Li^+ effect on the unit cell parameters remains inconsistent. Increased Li^+ doping, by way of higher concentrations of Li_2NO_3 in the precursor solutions, in hydroxyapatite nanoparticles resulted in a smaller unit cell volume and reduced *a* and *c* parameters [40]. In contrast, other findings demonstrated minimal differences in lattice parameters at 900 and 1200 °C but indications of reduced *a* and *c* parameters and a smaller unit cell volume at 1400 °C [41]. Li^+ possess a smaller ionic radii compared to calcium ions (0.076 and 0.100 nm in a 6-fold coordination) and therefore, are capable of substitution with calcium ions at either the Ca (I) or Ca(II) site, and reduce the unit cell volume [42]. The similarity in unit cell parameters between the Li 0 and Li 0.25 samples, and the similar carbonate contents in these samples, suggests that carbonate and not Li^+ is the main controller of change in the unit cell dimensions. The Li 1 sample does show a notable decrease in both unit cell parameters, but the specific role of Li^+, A-type or B-type carbonate substitution on this change can not be inferred here.

The Li^+ contents of the samples were close to their design values, and the equal exposure to carbonate/CO_2 during synthesis and heating, except for the additional carbonate in the Li_2CO_3 for the Li^+ substituted compositions, resulted in Li 0 and Li 0.25 having comparable carbonate contents, but the Li 1 sample having a much higher carbonate content that was consistent with the design composition. The similarity in all measured parameters for Li 0 and Li 0.25, except the Li^+ content, provides a good pair of samples to test the effect of Li^+ specifically on cell response. Equally, the Li 1 sample has a significantly larger Li^+ and carbonate content than the other two samples, but most of the physical parameters were comparable.

Thermal decomposition of Li 1 samples was observed at higher temperatures, above the 750 °C used here, evidenced with physical bloating of the samples, from the density and contact angle measurements (data not shown). These findings are consistent with previous data which indicated carbonated hydroxyapatite decomposition occurred at higher temperatures and with increased carbonate content [43]. Thus, fabricated discs were heated to attain 70–75 % sintered densities to prevent this change in morphology. Although a small calcite impurity phase was observed in the Li 1 sample, the consequence of this on subsequent cell response is considered minimal due to the relative low solubility of this phase.

In hydrolytic dissolution studies, investigations into mechanisms of hydroxyapatite dissolution indicated sequential processes of calcium and phosphate dissolution [44]. On the other hand, cell-mediated dissolution tends to occur more rapidly presumably due to the secreted acidic metabolites and enzymes [45]. This was previously illustrated in a comparison between porous Li^+ doped hydroxyapatite soaked in SBF and osteoblast biodegradation experiments [17]. In general, experimental data indicated greater solubility and thus, ion dissolution with Li 1 compared to Li 0.25 and Li 0 samples. This increase was likely due to the lower crystallinity and greater surface area in Li 1 samples. Previous studies have shown greater accumulative phosphate release in Li^+ doped hydroxyapatite compared to non-doped samples [17,19]. Likewise, prior investigations have established greater solubility with carbonate substitution [5,46].

Findings from the cell adhesion experiments demonstrated the impact of the varied surface topography on initial cell-material interaction with accelerated spreading on Li 1 discs. These findings were demonstrated in hOB cells and hMSCs and hence, were not considered a cell-dependent response. Earlier studies have illustrated the influence of microporosity, roughness, stiffness, surface charge, and wettability on protein adsorption [47]. Regarding the sintered discs analysed for *in vitro* experiments, the contact angle approximated to 60° with minute but insignificant changes between the different compositions. Therefore, the cell spreading differences observed with Li 1 discs are thought to be a result of factors other than surface wettability. Investigations into cell

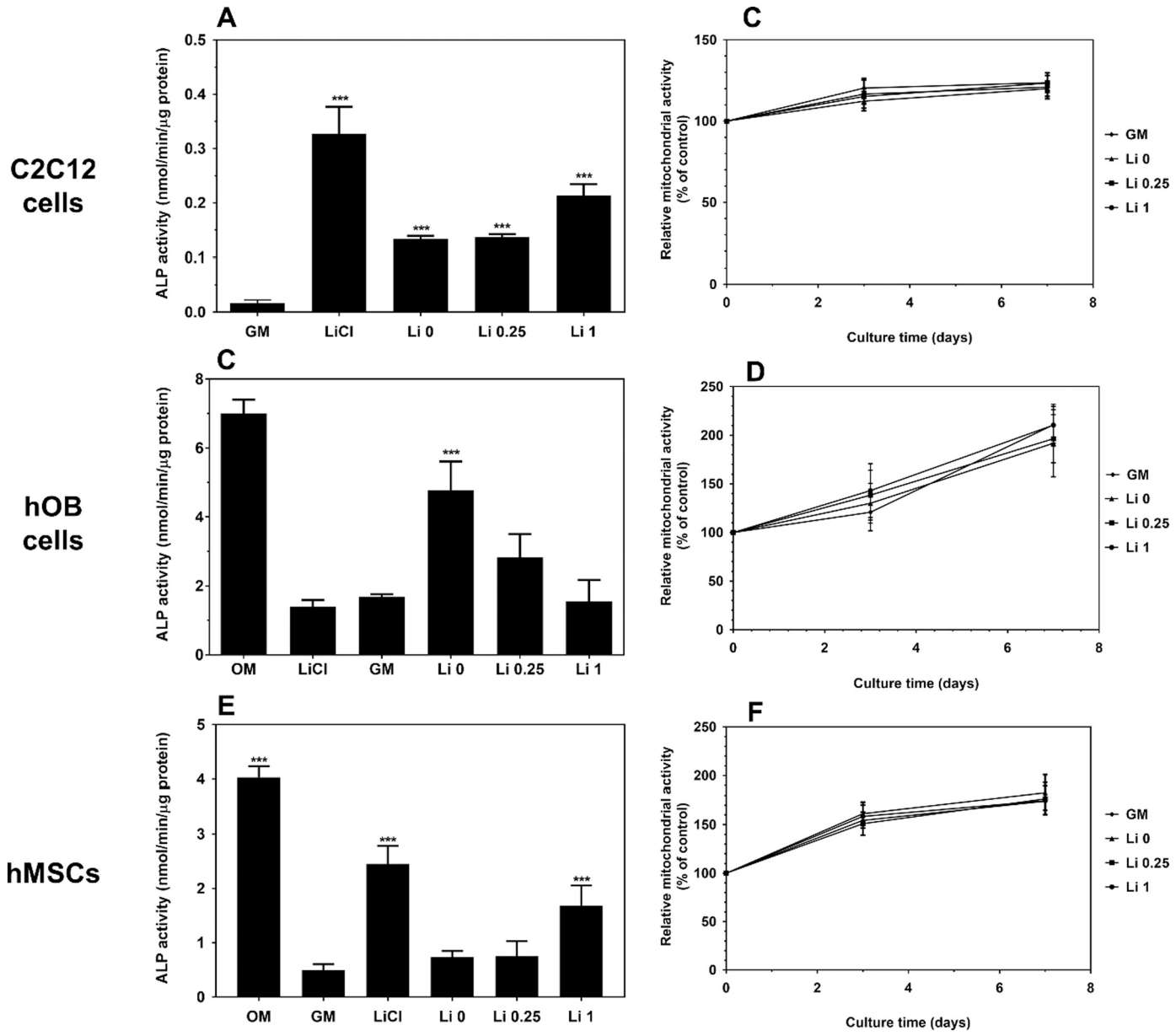

Fig. 8. ALP (A, C, E) and relative mitochondrial activity (C, D, F) of C2C12 cells, hOB cells, and hMSCs cultured on Li 0, Li 0.25, and Li 1 discs for 7 days.

adhesion on Li^+ doped hydroxyapatite remain scarce. A prior study reported improved MG63 cell adhesion and growth on Li^+ doped hydroxyapatite porous discs compared to the Li^+ free hydroxyapatite [17]. The authors speculated this was caused by a more compact bulk density in the Li^+ doped discs, in addition to the Li release to support proliferation. However, observations were made at later timepoints (day 4, 14, and 21) which failed to capture cell morphology during initial attachment.

Whilst initial cell attachment is predominantly dictated by the underlying surface features, the ion release from calcium phosphate samples influence the ensuing cell proliferation and differentiation. Nevertheless, the surface topography remains a crucial regulator of proliferation and specifier of lineage commitment [48–51]. Findings from the resazurin assays indicated the sintered discs maintained cytocompatibility for the 7-day culture period but induced no noticeable changes in cell proliferation. These responses differed from previous studies which demonstrated increased MG63 cell proliferation, as measured by the MTT assay, seeded on porous low Li^+-doped hydroxyapatite (99.5:0.5 Ca^{2+}:Li^+ molar ratio) [17]. Similar findings were observed in hFOB cells on Li^+ doped β-tricalcium phosphate discs [22]. In contrast, no significant differences were observed in hMSC proliferation on Li^+ doped β-tricalcium phosphate discs compared to the non-doped controls, in agreement with findings from this study [20]. Differences in Li^+ release, surface topography, and culture conditions are presumably attributable for these discrepancies.

Owing to the capacity for osteoinduction in response to the surface topography, surface chemistry, and dissolution products, a series of experiments were performed to assess these effects. In hOB cells, the osteogenic role of the surface topography was illustrated with the promotion of ALP activity on the sputter coated discs and the absence of differences in ALP activity on polished discs. Although not statistically significant, an increase in ALP activity was observed in sputter coated Li 1 discs compared to the unresponsiveness of hOB cells seeded onto uncoated Li 1 discs. Taken together, these findings would indicate that exposure to Li^+, either from the surface chemistry or material dissolution, impaired ALP activity of hOB cells. These results are in agreement with those obtained previously in hFOB cells on Li^+ doped hydroxyapatite pellets [15]. At lower Li^+ doping, hFOB cells remained

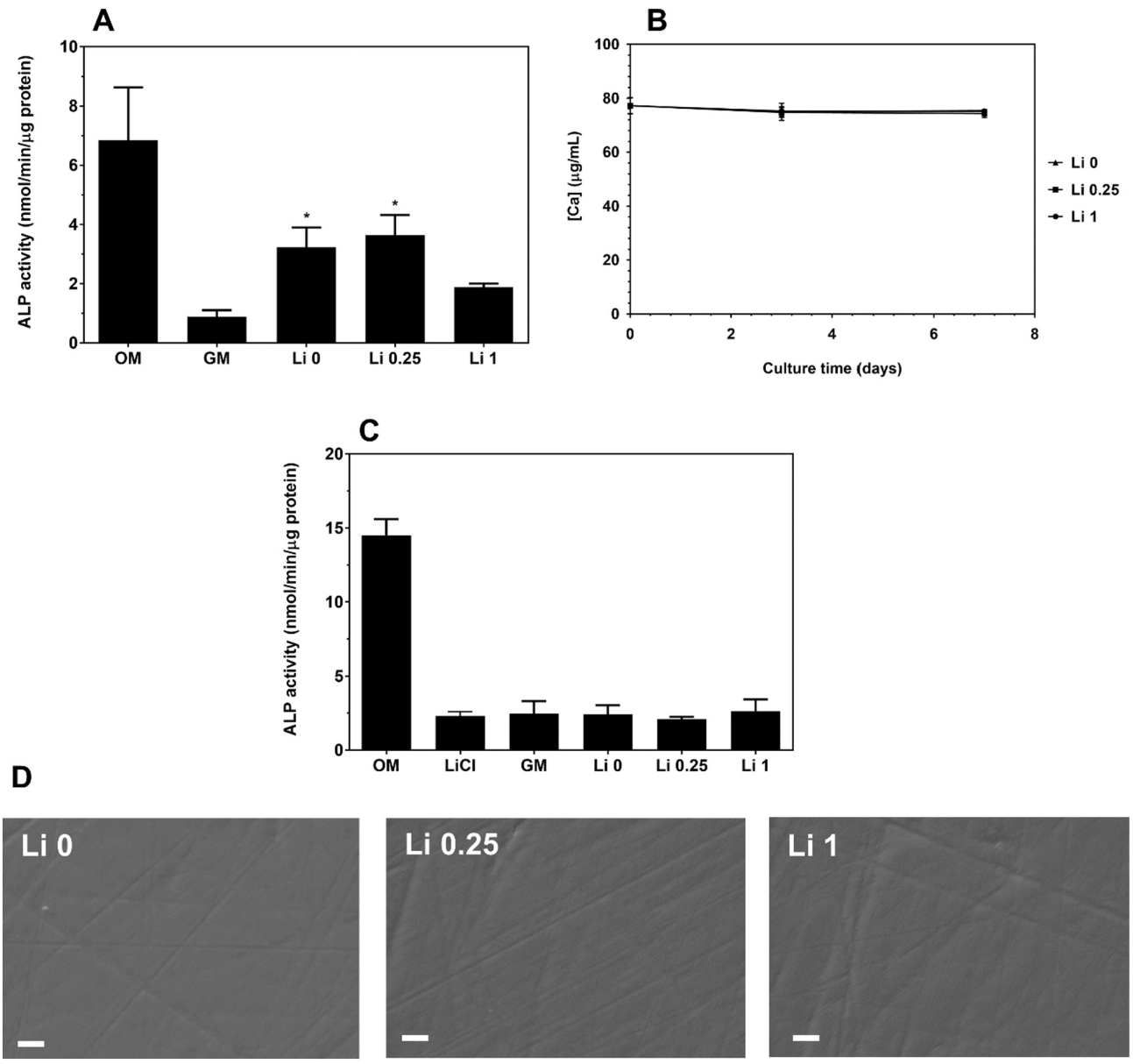

Fig. 9. ALP activities of hOB cells on sputter coated discs (A) with corresponding measurement of Ca concentration in the media (B) and on polished discs (C) with corresponding SEM micrographs of the disc surface following polishing (D).

unresponsive, whilst, a higher doping (2 wt%) resulted in impaired ALP production and secretion. In addition, the authors observed different degrees of impairment with sintering temperature which despite the absence of topography visualisation, would indicate a function of the topography on ALP production and secretion [15]. Moreover, the osteogenic potential of the surface topography was observed in C2C12 cells and hMSCs with upregulation of ALP activity in Li 0 discs compared to cells in the growth media control. On the other hand, the osteogenic role of Li^+ release was established in C2C12 cells exposed to Li 1 granules and conditioned media of Li 1 powders which were further authenticated in hMSCs. Determination of Li^+ content of the Li 1 powder conditioned media indicated hMSCs were exposed to a concentration of approximately 100 μg/mL (Fig. 6D); of note, 10 mM LiCl constitutes a Li^+ concentration of approximately 70 μg/mL. Whilst these experiments remove the influence of the surface topography, other factors such as changes in calcium and phosphate concentrations may influence cell differentiation. Typically, increased supplementation of calcium and inorganic phosphate have resulted in enhanced osteogenic differentiation [52–55]. Although the effects of calcium and phosphate release/depletion are capable of confounding findings, several lines of evidence would suggest this not to be the case. Measurement of calcium concentrations in the conditioned media indicated depletion with Li 0.25 granules and Li 0 and Li 0.25 powders, in addition to Li 1 samples, yet no differences in ALP activity were observed (Fig. 5B). Separately, calcium concentration of conditioned media remained comparable despite increasing mass of soaked Li 1 powders though disparate outcomes in ALP activity was measured (Fig. 5D). On the other hand, the elevated calcium release in Li 0 granules compared to Li 1 granules during culture failed to induce an increase in ALP activity (Fig. 5F). Thus, these findings would reasonably suggest Li^+ as the prime driver of osteogenic differentiation. The osteogenic role of the dissolution products derived from Li 1 samples was in accordance with prior investigations into Li^+ doped calcium phosphate cements using MG63 and MC3T3-E1 cells [21,56]. In addition, other investigations have shown similar trends in calcium/phosphate levels during culture with comparable osteogenesis in response to Li^+ doped samples [18,20].

The observed effects of Li^+ ions released from the compositions studied on the ALP activity of hMSCs and C2C12 cells, but not hOB cells, are consistent with the effect of Li^+ ions introduced from LiCl added to the media, as observed as a control in our studies, but also from published studies adding LiCl [11,12]. How this would translate to bone formation would need to be tested in a preclinical model, but this was out with the scope of this study. Although Li^+ ions released from samples did not appear to enhance the ALP activity of hOB cells, the surface topography of all samples did appear to enhance ALP activity when hOB cells were seeded on sintered discs, and this effect was inversely related to the level of lithium substitution. Although all compositions were prepared to have comparable sintered densities, the loss of this effect on ALP activity when sintered discs were polished suggests that distinct surface microstructures existed for each composition after sintering that altered cell response. The significance of this would depend on these different surface structures being produced in more relevant sample forms, such as macroporous scaffolds.

5. Conclusions

This study set out to synthesise and characterise a novel, charge balanced, Li^+ doped carbonated hydroxyapatite material with follow-up *in vitro* studies to evaluate suitability as a bone graft or scaffold. Findings demonstrated successful synthesis of carbonated hydroxyapatite with relatively low and high Li^+ substitutions. Furthermore, Li 1 samples were shown to possess improved sinterability, enhanced dissolution, and a disparate microstructure compared to Li 0 and 0.25 samples. *In vitro* assessment indicated favourable cell attachment and cytocompatibility for all the compositions evaluated. In addition, Li 1 samples demonstrated augmented osteoinduction in C2C12 cells and hMSCs in response to direct seeding onto discs, granules held within inserts, and conditioned media from soaked powders. Of interest, experiments using the non-LiCl responsive hOB cells indicated a functional role of the surface topography with a potential compounded effect from the surface chemistry.

Supplementary data to this article can be found online at https://doi.org/10.1016/j.bioadv.2022.213068.

CRediT authorship contribution statement

Nasseem Salam: Investigation, experimental data acquisition, data analysis, writing - original draft.

Iain R Gibson: Conceptualization, resources, experimental data acquisition and analysis (FTIR, surface area), supervision, funding acquisition, writing - review & editing, approving final draft.

Declaration of competing interest

The authors declare no conflict of interest related to the submitted work.

Acknowledgments

The authors would like to acknowledge the Microscopy and Histology Core Facility at the University of Aberdeen for support in this work, and Mr. Colin Taylor at the School of Geosciences for assistance in the combustion analysis. The authors thank the Institute of Medical Sciences, University of Aberdeen for funding (PhD studentship for NS) and the Royal Commission for the Exhibition of 1851 for funding contributions to this study.

References

[1] C. Cardemil, I. Elgali, W. Xia, et al., Strontium-doped calcium phosphate and hydroxyapatite granules promote different inflammatory and bone remodelling responses in normal and ovariectomised rats, PLoS One 8 (2013), e84932.
[2] L. Deng, D. Li, Z. Yang, et al., Repair of the calvarial defect in goat model using magnesium-doped porous hydroxyapatite combined with recombinant human bone morphogenetic protein-2, Biomed. Mater. Eng. 28 (2017) 361–377.
[3] R.F.B. Resende, G.V.O. Fernandes, S.R.A. Santos, et al., Long-term biocompatibility evaluation of 0.5 % zinc containing hydroxyapatite in rabbits, J. Mater. Sci. Mater. Med. 24 (2013) 1455–1463.
[4] K.A. Hing, P.A. Revell, N. Smith, T. Buckland, Effect of silicon level on rate, quality and progression of bone healing within silicate-substituted porous hydroxyapatite scaffolds, Biomaterials 27 (2006) 5014–5026.
[5] J. Barralet, S. Best, W. Bonfield, Carbonate substitution in precipitated hydroxyapatite: an investigation into the effects of reaction temperature and bicarbonate ion concentration, J. Biomed. Mater. Res. 41 (1998) 79–86.
[6] M. Wei, J.H. Evans, T. Bostrom, L. Grøndahl, Synthesis and characterization of hydroxyapatite, fluoride-substituted hydroxyapatite and fluorapatite, J. Mater. Sci. Mater. Med. 14 (2003) 311–320.
[7] J.T.B. Ratnayake, M. Mucalo, G.J. Dias, Substituted hydroxyapatites for bone regeneration: a review of current trends, J Biomed Mater Res B Appl Biomater 105 (2017) 1285–1299.
[8] A. Ressler, A. Žužić, I. Ivanišević, et al., Ionic substituted hydroxyapatite for bone regeneration applications: a review, Open Ceram. 6 (2021), 100122.
[9] I. Lodoso-Torrecilla, R. Klein Gunnewiek, E.C. Grosfeld, et al., Bioinorganic supplementation of calcium phosphate-based bone substitutes to improve: in vivo performance: a systematic review and meta-analysis of animal studies, Biomater. Sci. 8 (2020) 4792–4809.
[10] M. Arioka, F. Takahashi-Yanaga, M. Sasaki, et al., Acceleration of bone regeneration by local application of lithium: wnt signal-mediated osteoblastogenesis and wnt signal-independent suppression of osteoclastogenesis, Biochem. Pharmacol. 90 (2014) 397–405.
[11] N.K. Satija, D. Sharma, F. Afrin, et al., High throughput transcriptome profiling of lithium stimulated human mesenchymal stem cells reveals priming towards osteoblastic lineage, PLoS One 8 (2013), e55769.
[12] P. Clément-Lacroix, M. Ai, F. Morvan, et al., Lrp5-independent activation of wnt signaling by lithium chloride increases bone formation and bone mass in mice, Proc. Natl. Acad. Sci. U. S. A. 102 (2005) 17406–17411.
[13] V. Stambolic, L. Ruel, J.R. Woodgett, Lithium inhibits glycogen synthase kinase-3 activity and mimics wingless signalling in intact cells, Curr. Biol. 6 (1996) 1664–1669.
[14] C. Hartmann, A wnt canon orchestrating osteoblastogenesis, Trends Cell Biol. 16 (2006) 151–158.
[15] A.P.M. Shainberg, P. Valério, A. Zonari, Attachment and proliferation of osteoblasts on lithium-hydroxyapatite composites, Adv. Mater. Sci. Eng. 2012 (2012).
[16] M.A. Fanovich, M.S. Castro, J.M.P. Lopez, Improvement of the microstructure and microhardness of hydroxyapatite ceramics by addition of lithium, Mater. Lett. 33 (1998) 269–272.
[17] Y. Wang, X. Yang, Z. Gu, et al., In vitro study on the degradation of lithium-doped hydroxyapatite for bone tissue engineering scaffold, Mater. Sci. Eng. C 66 (2016) 185–192.
[18] D. Li, L. Huifang, J. Zhao, et al., Porous lithium-doped hydroxyapatite scaffold seeded with hypoxia-preconditioned bone-marrow mesenchymal stem cells for bone-tissue regeneration, Biomed. Mater. 13 (2018), 055002.
[19] Y. Luo, D. Li, J. Zhao, et al., In vivo evaluation of porous lithium-doped hydroxyapatite scaffolds for the treatment of bone defect, Biomed. Mater. Eng. 29 (2018) 699–721.
[20] P. Han, M. Xu, J. Chang, et al., Lithium release from β-tricalcium phosphate inducing cementogenic and osteogenic differentiation of both hPDLCs and hBMSCs, Biomater. Sci. 2 (2014) 1230.
[21] L. Li, R. Wang, B. Li, et al., Lithium doped calcium phosphate cement maintains physical mechanical properties and promotes osteoblast proliferation and differentiation, J Biomed Mater Res B Appl Biomater 105 (2017) 944–952.
[22] S. Vahabzadeh, V.K. Hack, S. Bose, Lithium-doped β-tricalcium phosphate: effects on physical, mechanical and in vitro osteoblast cell-material interactions, J Biomed Mater Res B Appl Biomater 105 (2017) 391–399.
[23] C.Q. Zhao, X.C. Xu, Y.J. Lu, et al., Doping lithium element to enhance compressive strength of β-TCP scaffolds manufactured by 3D printing for bone tissue engineering, J. Alloys Compd. 814 (2020), 152327.
[24] A. Bigi, G. Cojazzi, S. Panzavolta, et al., Chemical and structural characterization of the mineral phase from cortical and trabecular bone, J. Inorg. Biochem. 68 (1997) 45–51.
[25] J.H. Shepherd, D.V. Shepherd, S.M. Best, Substituted hydroxyapatites for bone repair, J. Mater. Sci. Mater. Med. 23 (2012) 2335–2347.
[26] C. Rey, B. Collins, T. Goehl, et al., The carbonate environment in bone mineral: a resolution-enhanced fourier transform infrared spectroscopy study, Calcif. Tissue Int. 45 (1989) 157–164.
[27] I.R. Gibson, S. Ke, S.M. Best, W. Bonfield, Effect of powder characteristics on the sinterability of hydroxyapatite powders, J. Mater. Sci. Mater. Med. 12 (2001) 163–171.
[28] ICDD PDF Card No. 9-432.
[29] E. Landi, A. Tampieri, G. Celotti, S. Sprio, Densification behaviour and mechanisms of synthetic hydroxyapatites, J. Eur. Ceram. Soc. 20 (2000) 2377–2387.
[30] A. Ito, Y. Sogo, A. Yamazaki, et al., Interlaboratory studies on in vitro test methods for estimating in vivo resorption of calcium phosphate ceramics, Acta Biomater. 25 (2015) 347–355.
[31] A.L.B. Maçon, T.B. Kim, E.M. Valliant, et al., A unified in vitro evaluation for apatite-forming ability of bioactive glasses and their variants, J. Mater. Sci. Mater. Med. 26 (2015) 115.

[32] T. Attin, K. Becker, C. Hannig, et al., Suitability of a malachite green procedure to detect minimal amounts of phosphate dissolved in acidic solutions, Clin. Oral Investig. 9 (2005) 203–207.
[33] H.-J. Prins, A.K. Braat, D. Gawlitta, et al., In vitro induction of alkaline phosphatase levels predicts in vivo bone forming capacity of human bone marrow stromal cells, Stem Cell Res. 12 (2014) 428–440.
[34] B. Han, B. Tang, M.E. Nimni, Quantitative and sensitive in vitro assay for osteoinductive activity of demineralized bone matrix, J. Orthop. Res. 21 (2003) 648–654.
[35] W. Bonfield, I.R. Gibson, Novel synthesis and characterization of an AB-type carbonate-substituted hydroxyapatite, J. Biomed. Mater. Res. 59 (2002) 697–708.
[36] M.E. Fleet, X. Liu, Coupled substitution of type a and B carbonate in sodium-bearing apatite, Biomaterials 28 (2007) 916–926.
[37] J.E. Barralet, S.M. Best, W. Bonfield, Effect of sintering parameters on the density and microstructure of carbonate hydroxyapatite, J. Mater. Sci. Mater. Med. 11 (2000) 719–724.
[38] H. Madupalli, B. Pavan, M.M.J. Tecklenburg, Carbonate substitution in the mineral component of bone: discriminating the structural changes, simultaneously imposed by carbonate in a and B sites of apatite, J. Solid State Chem. 255 (2017) 27–35.
[39] R. Zapanta-LeGeros, Effect of carbonate on the lattice parameters of apatite, Nature 206 (1965) 403–404.
[40] V.P. Padmanabhan, T.S.N. Sankara Narayanan, S. Sagadevan, et al., Advanced lithium substituted hydroxyapatite nanoparticles for antimicrobial and hemolytic studies, New J. Chem. 43 (2019) 18484–18494.
[41] V. Smirnov, S. Smirnov, A. Krylov, et al., Influence of lithium on the structure and phase composition formation in the synthesis of hydroxyapatite, Dokl. Chem. 481 (2018) 177–180.
[42] R.D. Shannon, Revised effective ionic radii and systematic studies of interatomic distances in halides and chalcogenides, Acta Crystallogr. Sect. A 32 (1976) 751–767.
[43] J. Barralet, J.C. Knowles, S. Best, W. Bonfield, Thermal decomposition of synthesised carbonate hydroxyapatite, J. Mater. Sci. Mater. Med. 13 (2002) 529–533.
[44] S.V. Dorozhkin, Surface reactions of apatite dissolution, J. Colloid Interface Sci. 191 (1997) 489–497.
[45] C.E. Holy, S.M. Dang, J.E. Davies, M.S. Shoichet, In vitro degradation of a novel poly(lactide-co-glycolide) 75/25 foam, Biomaterials 20 (1999) 1177–1185.
[46] A. Porter, N. Patel, R. Brooks, et al., Effect of carbonate substitution on the ultrastructural characteristics of hydroxyapatite implants, J. Mater. Sci. Mater. Med. 16 (2005) 899–907.
[47] C.J. Wilson, R.E. Clegg, D.I. Leavesley, M.J. Pearcy, Mediation of biomaterial-cell interactions by adsorbed proteins: a review, Tissue Eng. 11 (2005) 1–18.
[48] A.J. Engler, S. Sen, H.L. Sweeney, D.E. Discher, Matrix elasticity directs stem cell lineage specification, Cell 126 (2006) 677–689.
[49] B.J. Papenburg, E.D. Rodrigues, M. Wessling, D. Stamatialis, Insights into the role of material surface topography and wettability on cell-material interactions, Soft Matter 6 (2010) 4377–4388.
[50] Y. Yang, K. Wang, X. Gu, K.W. Leong, Biophysical regulation of cell behavior—cross talk between substrate stiffness and nanotopography, Engineering 3 (2017) 36–54.
[51] G. Abagnale, M. Steger, V.H. Nguyen, et al., Surface topography enhances differentiation of mesenchymal stem cells towards osteogenic and adipogenic lineages, Biomaterials 61 (2015) 316–326.
[52] Y. Sai, Y. Shiwaku, T. Anada, et al., Capacity of octacalcium phosphate to promote osteoblastic differentiation toward osteocytes in vitro, Acta Biomater. 69 (2018) 362–371.
[53] M.N. Lee, H.S. Hwang, S.H. Oh, Elevated extracellular calcium ions promote proliferation and migration of mesenchymal stem cells via increasing osteopontin expression, Exp. Mol. Med. (2018) 50.
[54] S. Ali Akbari Ghavimi, B.N. Allen, J.L. Stromsdorfer, et al., Calcium and phosphate ions as simple signaling molecules with versatile osteoinductivity, Biomed. Mater. 13 (2018), 055005.
[55] C.B.S.S. Danoux, D.C. Bassett, Z. Othman, et al., Elucidating the individual effects of calcium and phosphate ions on hMSCs by using composite materials, Acta Biomater. 17 (2015) 1–15.
[56] L. Li, X. Peng, Y. Qin, et al., Acceleration of bone regeneration by activating Wnt/β-catenin signalling pathway via lithium released from lithium chloride/calcium phosphate cement in osteoporosis, Sci. Rep. 7 (2017) 45204.